Signature of charge migration in modulations of double ionization

François Mauger,[1,*] Paul M. Abanador,[1] Adam Bruner,[2] Adonay Sissay,[2] Mette B. Gaarde,[1] Kenneth Lopata,[2] and Kenneth J. Schafer[1]

[1]*Department of Physics and Astronomy, Louisiana State University, Baton Rouge, Louisiana 70803-4001, USA*

[2]*Department of Chemistry, Louisiana State University, Baton Rouge, Louisiana 70803-4001, USA*

(Received 28 November 2017; published 9 April 2018)

We present a theoretical investigation of charge migration following strong-field ionization in a multielectron system. We study a model homonuclear molecule with two electrons, each restricted to one dimension ($1+1D$), interacting with a strong, static electric field. We show that in this system charge migration results from the interplay between multiple ionization channels that overlap in space, creating a coherent electron-hole wave packet in the cation. We also find that, in our case, charge migration following the first ionization manifests as a modulation of the subsequent double-ionization signal. We derive a parametrized semiclassical model from the full multielectron system and we discuss the importance of the choice of cation electronic-structure basis for the efficacy of the semiclassical representation. We use the *ab initio* solution of the full $1+1D$ system as a reference for the qualitative and quantitative results of the parametrized semiclassical model. We discuss the extension of our model to long-wavelength time-dependent fields with full-dimension, many-electron targets.

DOI: 10.1103/PhysRevA.97.043407

I. INTRODUCTION

With the progress in ultrafast laser technology, strong-field physics is now able to probe the structure and dynamics of matter at the space and time scale of the electron [1–7]. For time-resolved analyses, the temporal coherence of the laser electric field defines an intrinsic clock, with a period of a few femtoseconds in the near- to midinfrared regime [8–15]. For instance, in a linearly polarized laser field, recollision events [16,17]—where a previously ionized electron revisits its parent cation—define a subcycle reference associated with the different recollision trajectories [18,19] and, therefore, with subfemtosecond resolution in the infrared. Bringing together high temporal and spatial resolution for the "real-time" observation of electron dynamics has long been a goal of ultrafast physics. In this context, the observation and analysis of the phenomena of charge migration have attracted a lot of attention recently [20–27]. Charge migration is the coherent, correlation-driven, purely electronic dynamic immediately following the excitation or ionization of a molecule, before the nuclei have had time to move. It has been widely speculated that the attosecond electron dynamics can play a crucial role in the longer-time-scale phenomena like charge transfer and bond rearrangement, which implies that the control of attosecond dynamics can determine such chemical processes [21,28].

Coherence and correlation are at the core of strong-field physics, especially given that the initial systems are usually atoms or molecules in their ground state. For instance, nonsequential double ionization [29–32]—and its "knee" signature, which exceeds simple sequential ionization predictions by orders of magnitudes—spotlights the central role of electron correlation in strong-field processes [33–35]. Further analyses of the dynamics have revealed a rich variety in the pathways leading to nonsequential double ionization [36–38]. Laser-induced electron diffraction [39]—exploiting the *in situ* coherent probe of a preionized electron scattering on its parent ion—has been used to retrieve the nuclear geometric structure of molecular compounds [40,41]. Alternatively, still using the intrinsic coherence of strong-field laser-matter interaction, direct imaging of the electronic structure has been performed with tomographic reconstruction of molecular orbitals [42–44]. Even without recollision, strong-field ionization studies have proven a powerful probe of the electronic structure and properties of matter [9,45,46].

In this article, we present a theoretical and numerical investigation of charge migration following strong-field multichannel ionization. We consider a model homonuclear molecule with two electrons, each restricted to one dimension ($1+1D$), interacting with a strong, static electric field. Somewhat counterintuitively we find the dynamics in such a static field physically enlightening, despite the absence of any explicit time dependence. Indeed, the removal of a first electron by the field starts a molecular clock in the cation which can be probed later, e.g., with the ionization of a second electron. We show that the charge migration results from the interplay between multiple ionization channels that overlap in space, i.e., a coherent electron-hole wave packet in the cation. In our $1+1D$ system, we identify a signature of the cation charge migration dynamics, a modulation of the subsequent double-ionization signal. From the full multielectron system, we derive a parametrized semiclassical model where the hypotheses and approximations leading to the analytical prediction are identified. Of all the ionization and molecular parameters in the model, we highlight the importance of the cation electronic-structure basis for the efficacy of the semiclassical representation. We validate the model, qualitatively and quantitatively, against reference *ab initio* solutions of the full

*fmauger@phys.lsu.edu

$1+1D$ system. We discuss the extension of our parametrized semiclassical model to long-wavelength oscillating laser fields with full-dimension, many-electron targets.

For realistic polyatomic molecules, brute-force *ab initio* solutions of the full time-dependent Schrödinger equation (TDSE) are out of analytical and computational reach. As an alternative, one could turn to quantum-chemical techniques like time-dependent density functional theory (TDDFT) [47–52]. Such an approach, however, faces two fundamental difficulties: (i) the validity of the chosen exchange-correlation functional in the nonlinear regime and (ii) the interpretation of correlation-driven charge migration dynamics in a framework that treats electrons as virtually independent particles. As a second alternative, one could stick to the TDSE framework and break the problem into smaller components, corresponding to the key elements of the charge migration, and piece them together with relevant system parameters [53,54]. Such approaches are built to facilitate the analysis and interpretation of the process, but they also suffer from fundamental difficulties of their own: (i) the determination of the model parameters and (ii), even assuming that these are perfectly known, the intrinsic precision of the semiclassical approximation. Here we take advantage of the simplicity of our $1+1D$ model to address the second difficulty, as one can perform brute-force integration of the full TDSE, for reference, and all ionization and molecular parameters can be computed with a high precision.

The paper is organized as follows: Section II introduces some key concepts of our analysis of charge migration, and its signature in the modulation of double ionization, in a static field from the point of view of classical mechanics. Section III introduces our quantum model and theoretical treatment of multichannel ionization. Section IV details the derivation of the corresponding semiclassical model. Section V applies it to the analysis of our $1+1D$ model and the signature of charge migration in double ionization. Finally, in Sec. VI we conclude the paper, summarizing the key findings and discussing perspectives for real systems and real laser fields. Unless otherwise specified, we use atomic units (a.u.) throughout the paper.

II. MODULATION OF DOUBLE IONIZATION AS A SIGNATURE OF CHARGE MIGRATION

Although we are ultimately interested in the full quantum ionization dynamics, it is useful to first look at the classical limit, where the Coulomb interaction with the core and other electrons is negligible (strong-field approximation). Following ionization, the dynamics of an electron in a static electric field of amplitude $\mathcal{E}$ can be solved for analytically,

$$r(\tau_{\rm cl}) = -\frac{\mathcal{E}}{2}\tau_{\rm cl}^2 \Leftrightarrow \tau_{\rm cl} = \sqrt{\left|\frac{2r}{\mathcal{E}}\right|}, \tag{1}$$

assuming that the electron is initially at the origin and with zero velocity. Here we are most interested in the reciprocal part of the equation: Static fields spatially separate electrons based on the delay since ionization $\tau_{\rm cl}$ and the ionization distance r can be seen as a time axis. The use of static dc fields elides *two* types of interferences that would be present in their ac counterparts: (i) the cycle-to-cycle interference responsible for individual peaks in the above-threshold ionization and high-harmonic-generation spectra and (ii) the subcycle interference of quantum paths leading to the same observable [19], e.g., direct and backscattered photoelectrons in above-threshold ionization and short and long trajectories in high-harmonic generation.

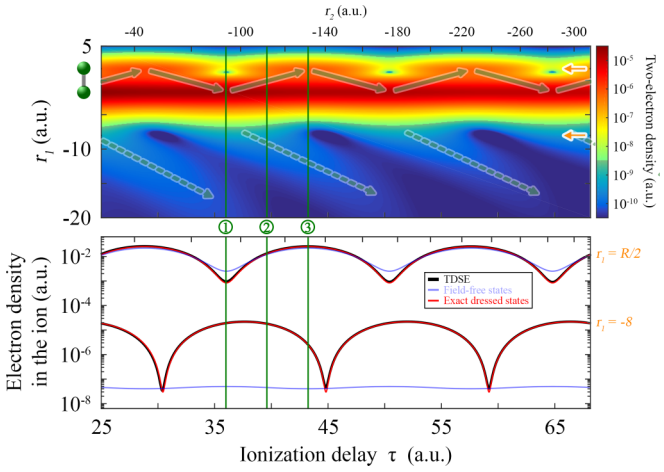

FIG. 1. Upper panel: Two-electron density $|\psi(r_1,r_2)|^2$ for our full $1+1D$ TDSE simulations. In the molecular model we set the internuclear distance $R = 3.5$ a.u., the electron-nucleus/electron-electron softening parameter $a_{en}/a_{ee} = 0.5/1$, effective charge $Z = 1$, and static electric-field amplitude $\mathcal{E} = 0.13$ a.u. Solid arrows label the charge migration between the two molecular centers, following the first multichannel ionization event. Dashed arrows represent the subsequent double-ionization bursts, as signatures of the charge migration in the cation. Lower panel: Comparison of the electron density in the cation, (15), for selected r_1 sections (labeled with small arrows in the upper panel) of the TDSE and semiclassical models, (13). The ionization delay τ used here is defined in Eq. (14). For a qualitative understanding, its classical limit introduced in Eq. (1) can be used instead.

Now consider (sequential) double ionization in the same static field. The arguments of Eq. (1) can be applied to each electron coordinate r_1 and r_2 individually. This means that the analysis of the *spatially* correlated two-electron density gives us information about the *dynamics* following the first ionization event and eventually leading to the second ionization. An illustration of that analysis is displayed in the upper panel in Fig. 1, where the density has been obtained from our $1+1D$ model wave function $|\psi(r_1,r_2)|^2$ (defined later). In the lower part of the panel we observe diagonal "stripes" in the density (highlighted with dashed arrows), which we therefore identify as a modulation of the double-ionization signal with respect to $\tau_{\rm cl}$. Interestingly, in the upper part of the panel, we note that this modulation is synchronized with another type of density motion, between the two centers of the molecule (solid diagonal arrows). Later we show that this corresponds to a migration of the charge in the cation following multichannel ionization and that the modulation of the double-ionization signal is a signature of that charge migration dynamics.

III. MODEL

We consider the quantum-mechanical dynamics of an N-active electron system, as described by the TDSE,

$$i\partial_t \psi(\mathbf{r}^N;t) = \hat{\mathcal{H}}_N(\mathbf{r}^N)\psi(\mathbf{r}^N;t), \tag{2}$$

in the presence of a static electric field of amplitude $\mathcal{E}$. Here $\hat{\mathcal{H}}_N$ and $|\psi\rangle$ are the Hamiltonian operator and total N-electron wave function, respectively. For simplicity we use $\mathbf{r}^N$ as a short-hand notation for the multielectron coordinates $r_1,\ldots,r_N$.

A. Molecular model for numerical simulations

For numerical simulations we consider the simplest system that fulfills the requirements for charge migration following ionization discussed in Sec. I. It is given by the $1+1D$ soft-Coulomb potential [55]

$$\hat{\mathcal{V}}(r_1,r_2) = -\frac{Z}{\sqrt{\left(r_1 \pm \frac{R}{2}\right)^2 + a_{en}^2}} - \frac{Z}{\sqrt{\left(r_2 \pm \frac{R}{2}\right)^2 + a_{en}^2}} + \frac{1}{\sqrt{(r_1-r_2)^2 + a_{ee}^2}}, \tag{3}$$

where a_{en} and a_{ee} are the electron-nucleus and electron-electron softening parameters, respectively. This model is simple enough to allow for full *ab initio* TDSE computations, to serve as a reference in quantitative analysis, and yet it is complex enough to exhibit multichannel ionization and subsequent charge migration in the cation. For all figures shown here, we take the internuclear distance $R = 3.5$ a.u. (1.9 Å), effective charge $Z = 1, a_{en}/a_{ee} = 0.5/1$, and static-field amplitude $\mathcal{E} = 0.13$ a.u. (the same amplitude as an ac field with an intensity of 6×10^{14} W/cm^2). For reference, with these parameters the energy difference between the (dressed) ionization channels is about 12 eV, which gives the period of about 14.5 a.u. (about 350 as) for the charge migration observed in the cation. We note that full-dimensional molecular systems with closely spaced energy states generally can be dipole coupled with much lower field amplitudes than considered here.

In order to discriminate between the channels, we consider a system with two spatially different orbitals and so use the lowest-energy triplet state as the initial condition. In the dipole approximation the $1+1D$ Hamiltonian operator $\mathcal{H}_2$ in Eq. (2) preserves the (anti)symmetry of the initial condition, which prevents any leakage to a lower-lying symmetric state. From the practical point of view, it also means that one needs only to record the ionization wave function in one of the two electron coordinates. We choose r_2 as this coordinate and absorb the outgoing wave function along the other electronic coordinate.

In numerical simulations we first smoothly ramp up the field from the (field-free) triplet initial state to reach the desired static-field amplitude. All numerical analyses are performed after a sufficient static-field duration such that all transient effects associated with the ramp-up have moved outside of the simulation box. We have checked the robustness of our results with the ramp-up and static-field durations, field strength, and molecular and discretization parameters. Later we use the result of these *ab initio* full TDSE simulations as a reference against which parametrized semiclassical models can be quantitatively tested.

B. Single-ionization effective model

In the physical picture of the TDSE, (2), single ionization corresponds to portions of the wave function elongated in exactly one electronic coordinate, e.g., r_N, while the other ($\mathbf{r}^{N-1}$) remain localized. In such regions, the dynamics between the ionized and the cation electrons becomes decoupled and the total Hamiltonian operator splits into two effective ones [13,54]:

$$\hat{\mathcal{H}}_N(\mathbf{r}^N) \approx \hat{\mathcal{H}}_{N-1}(\mathbf{r}^{N-1}) + \hat{\mathcal{H}}_1(r_N). \tag{4}$$

In this formulation, we identify three components of the total wave function, which should be clearly distinguished. First is the neutral component—later labeled with the "n" superscript—with all N electron coordinates close to the core region and from which originates ionization. Next are the cation and ionized electron components, respectively, with $N-1$ and 1 electrons and described with the effective operators $\hat{\mathcal{H}}_{N-1}$ and $\hat{\mathcal{H}}_1$. Although they are *decoupled*, it is important to keep in mind that the dynamics of the cation and ionized electron components are still *correlated (entangled)*, through the ionization condition: Dynamically, they are both born out of the same neutral component at the time of ionization.

The decomposition, (4), is most interesting in that it naturally defines orthonormal representation bases for each subspace: The cation component can be expanded in a basis of $N-1$ electron states, which we generically denote $|\tilde{\psi}_k\rangle$ (here the tilde is used to discriminate the neutral, with N electrons, and the cation, with $N-1$ components). Throughout the paper, these correspond to our ionization channels. The most intuitive basis corresponds to the ionic-field-free eigenstates, labeled with a "0" superscript in what follows. In a single Slater determinant approximation, such states can be labeled by the orbital of the electron-hole. As we later show, other "smarter" choices of basis are also possible. On the other hand, the ionized electron component is described with a one-electron continuum, which we generically label $|v\rangle$. Depending on the degree of precision required, one can use, e.g., plane waves/Volkov states, Coulomb waves [56], and exact one-electron continuum states [57].

In the product basis, the total N-electron wave function, with ionization along the electronic coordinate r_N, therefore reads [22,58,59]

$$|\psi\rangle = e^{iI_p^n t}|\psi^n\rangle + \sum_{k=1}^{\tilde{N}} e^{iI_{p_k}t}\int \beta_k(v,t)|\tilde{\psi}_k\rangle\otimes|v\rangle\, dv. \tag{5}$$

Analytically, finding the coefficients β_k is equivalent to solving the problem. Here $|\psi^n\rangle$ is the neutral component, from which the single ionization originates, with total ionization potential I_p^n. Although it vanishes in the region of interest, this term is kept as a reminder of the correlation (entanglement) between the cation and the ionized electron components, through the initial ionization condition. I_{p_k} is the total ionization potential of the corresponding cation basis set component $|\tilde{\psi}_k\rangle$. In this representation $I_p^n - I_{p_k}$ is the vertical ionization energy to the channel k. $\tilde{N}$ is the truncation order in the cation basis expansion. Its actual value is largely system specific and depends, e.g., on the number of ionization channels, the cation component basis, and whether excited states are involved in the process of interest.

C. Retrieving channel populations

To obtain the population in a given ionization channel k we project the total wave function onto the corresponding cation

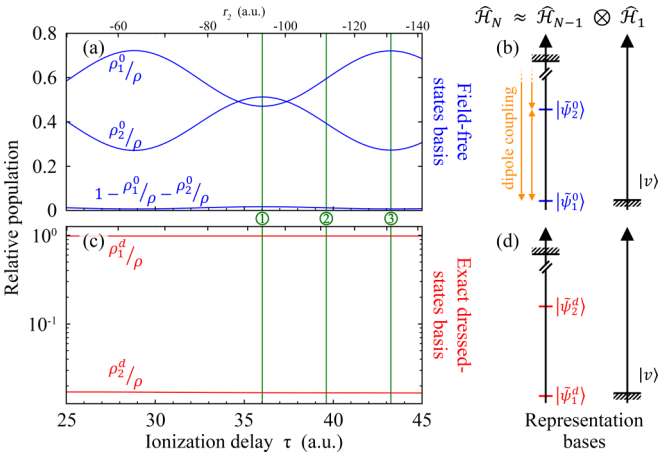

FIG. 2. Charge-migration dynamics and modeling following multichannel ionization by a strong static laser field. (a, c) The relative population ρ_k/ρ, as defined in Eqs. (6) and (7), extracted from full TDSE simulations for field-free and exact dressed-state cation bases, respectively. The ionization delay τ is defined with Eq. (14). For a qualitative understanding, its classical limit introduced in Eq. (1) can be used instead. (b, d) Differences between the two representation bases.

state as

$$\rho_k(r_N) = N|\langle\tilde{\psi}_k| \otimes \langle r_N|\psi\rangle|^2 = N\left|\int \beta_k(v)\langle r_N|v\rangle\, dv\right|^2 \quad (6)$$

from Eq. (5). In practice, this corresponds to taking a slice of the total N-electron wave function at a given ionization coordinate r_N, or equivalently a given ionization delay τ, and projecting the result onto the cation basis-state element. Here the prefactor N is introduced to cast the problem in a form similar to TDDFT, where all properties are functionals of the single-particle density [49]

$$\rho(r_N) = N\int |\psi(\mathbf{r}^{N-1},r_N)|^2\, d\mathbf{r}^{N-1}. \quad (7)$$

In Fig. 2(a) we display the relative populations, $\rho_k(r_N)/\rho(r_N)$, in the first two field-free states of the cation for our $1+1D$ molecular model of potential (3). Results are shown as a function of the ionization coordinate or, equivalently, the delay since the first ionization (see Sec. II). Because of the dipole coupling between the cation states [see Fig. 2(b)] we observe population transfer between them, which manifests through the oscillations in the curves. Alternatively, Figs. 2(c) and 2(d) display the populations in a "smart" exact dressed-state cation basis set [60–62]. In the dressed basis, the coupling between channels is effectively removed and the population in each of them is conserved over time.

The cation component basis closure, together with Eqs. (6) and (7), imposes the charge conservation condition

$$\rho = \sum_{k\geqslant 1}\rho_k.$$

Alternatively, one can use the charge conservation condition to determine the number of cation states to include in expansion (5), i.e., $\tilde{N}$, by tracking the residual population proportion $1-\sum_{k=1}^{\tilde{N}}\rho_k/\rho$.

IV. SEMICLASSICAL MODEL

With a static field and truncation of the cation component basis to order $\tilde{N}$ in Eq. (5), $\hat{\mathcal{H}}_{N-1}$ takes the form of a constant finite-dimensional Hermitian matrix, which we denote $\tilde{\mathcal{H}}_{N-1}$. We first diagonalize the matrix

$$\tilde{\mathcal{H}}_{N-1}|\tilde{\psi}_k^d\rangle = -I_{p_k}^d|\tilde{\psi}_k^d\rangle$$

and rewrite the problem in an orthonormal basis of eigenstates. Immediately, we see that the $I_{p_k}^d$ and $|\tilde{\psi}_k^d\rangle$ correspond to the *dressed* ionization potential and cation component state. Effectively, this decouples the dynamics of the dressed channels, which can be treated as virtually independent systems—with populations conserved in time—while fully retaining the dipole couplings with the external field. Here as well, it is important to keep in mind that, although decoupled, the dressed ionization channels remain correlated (entangled), through the multichannel ionization condition. In what follows, dressed states and associated parameters/quantities are labeled with a "d" superscript.

A. Approximate solution

With each dressed state behaving as an independent channel we follow the procedure of the Lewenstein model [18] and combine the wave function decomposition, (5), with the TDSE, (2), and effective Hamiltonian, (4). For illustration and similarly to Ref. [18], we consider a plane wave and strong-field approximation description of the continuum electron such that, in the length gauge, the dynamics is described by

$$i\dot{\beta}_k^d - \dot{v}r_N\beta_k^d = e^{i\left(I_p^n - I_{p_k}^d\right)t}d_k^d(v) + \frac{v^2}{2}\beta_k^d + \mathcal{E}r_N\beta_k^d$$

for each dressed channel. Here d_k^d is the (complex) transition element describing ionization from the neutral to the dressed ionization channel k, $|\psi^n\rangle \to |\tilde{\psi}_k^d\rangle \otimes |v\rangle$. The strong-field approximation imposes $\dot{v} = -\mathcal{E}$, and we solve the differential equation analytically [18],

$$e^{iI_{p_k}^d t}\int \beta_k^d(v,t)|\tilde{\psi}_k^d\rangle \otimes |v\rangle\, dv = -i\iint^t d_k^d(v(t_0))e^{iS_k^d[t_0,t,r_N,v]}\, dt_0 dv|\tilde{\psi}_k^d\rangle \otimes |\mathbb{I}_d\rangle, \quad (8)$$

where $|\mathbb{I}_d\rangle$ is the identity—the contribution from the continuum (plane-wave) $|v\rangle$ is included in the global phase term—and S_k^d is given by

$$S_k^d = I_{p_k}^d t + \left(I_p^n - I_{p_k}^d\right)t_0 - \int_{t_0}^t \frac{v(s)^2}{2}\, ds + vr_N, \quad (9)$$

with $v(s) = v + \mathcal{E}(t_0 - s)$. Beyond the present case of dc ionization, we note the similarity in the analytical solution above to other semiclassical treatments of multichannel/active electron systems in strong-field physics [7,23,25,54].

Physically, Eqs. (8) and (9) can be interpreted as the ionization time t_0 and initial velocity v required for a classical electron to reach the coordinate r_N at time t. Similarly,

$I^d_{p_k}(t-t_0)$ and $-\int_{t_0}^{t}\frac{v(s)^2}{2}\,ds$ are the phases accumulated by the dressed cation component k and ionized electron, respectively, following ionization. The term $I^n_p t_0$ ensures the synchronization of phases between the neutral and the ionization channel, at the instant of ionization, and the term vr_N is due to the spatial dependence of the continuum state.

More interestingly, in Eq. (8) we recognize the temporal factorization of the wave function in terms of the two steps of the ionization process: ionization, with $d^d_k(v(t_0))$, and propagation, with $e^{iS^d_k[t_0,t,r_N,v]}$. Here, for each dressed channel k, the result reads as a single-active-electron system would. Assuming that one can generalize the notion of such dressed states to oscillating fields (see Sec. VI), it opens a clear perspective for extending quantitative rescattering (QRS) results [63] and similar high-harmonic-generation spectrum factorization [64] to multichannel processes. This would be done by performing the temporal-to-frequency factorization [57] for each dressed channel independently and coherently summing all contributions. We stress that this is possible only because the dressed channels are virtually independent systems. Indeed, QRS factorization relies on the generality of the propagation component of the factorization, which is found to be very similar across targets. This property breaks down when population transfer (charge migration) happens between the different cationic states, e.g., as it does in the field-free cation-state basis.

B. Stationary phase approximation

With its multidimensional integrals, Eq. (8) is rather cumbersome for analyses of the charge migration dynamics. To simplify its expression we consider the familiar stationary phase approximation (SPA). Without loss of generality we assume that the static field is fully on at time $t=0$ and select a position r_N along the ionization direction and time $t \gtrsim \sqrt{|2r_N/\mathcal{E}|}$, (1), to avoid transient effects of the laser ramp-up. For each dressed channel, the SPA condition $\nabla S^d_k = 0$ is defined by the two equations

$$I^n_p - I^d_{p_k} + \frac{v^2}{2} = 0 \quad \text{and} \quad \int_{t_0}^{t} v + \mathcal{E}(t_0 - s)\,ds - r_N = 0. \tag{10}$$

By definition, the neutral ionization potential is larger than that of any of the cations, such that the SPA velocity is a purely imaginary number,

$$v = -i\sqrt{2\left(I^n_p - I^d_{p_k}\right)},$$

which is sometimes interpreted as a generalized energy conservation condition for ionization, extended to the complex plane. Then the second equation defines the corresponding SPA ionization time

$$t_0 = t - \frac{v + \sqrt{2\left(-\mathcal{E}r_N - I^n_p + I^d_{p_k}\right)}}{\mathcal{E}}.$$

This equation defines the classically forbidden region $r_N > -(I^n_p - I^d_{p_k})/\mathcal{E}$, assuming $\mathcal{E} > 0$, and corresponds to the picture of tunnel ionization through a barrier corresponding to the vertical ionization energy to channel k.

After additional calculations and simplifications, we find that the real part of the stationary phase is given by

$$S^s_k(r_N,t) = I^n_p t + \frac{\left[2\left(-\mathcal{E}r_N - I^n_p + I^d_{p_k}\right)\right]^{\frac{3}{2}}}{3\mathcal{E}}. \tag{11}$$

Alternatively, similar results can be obtained in parabolic coordinates, where the Coulomb potential plus static-field problem is separable [65,66]. Finally, following QRS-type arguments [63], we assume that the spatial profile along the ionization channel is generic and further factorize the wave function

$$|\psi\rangle = \sqrt{\frac{\rho(r_N)}{N}}\sum_{k=1}^{\tilde{N}} \gamma^d_k e^{i\left(S^s_k(r_N,t)+\Phi^d_k\right)}\left|\tilde{\psi}^d_k\right\rangle, \tag{12}$$

where γ^d_k is the proportion of ionization to, and Φ^d_k is the absolute ionization phase out of, the dressed channel k.

Interestingly, we note that Eq. (12) corresponds to a fully parametrized semiclassical (ionization) model, where the parameters are related to the physical/chemical ionization properties of each cation channel. Quantum-chemical methods such as TDDFT or Hartree-Fock theory provide means to obtain such parameters [23]. A detailed discussion about how these should be computed goes beyond the scope of the present paper.

V. NUMERICAL SIMULATIONS

We now turn to the $1+1D$ molecular system introduced in Sec. III A for a quantitative analysis of the parametrized semiclassical model of Eq. (12). In our $1+1D$ model, in Fig. 2(c) we see that most of the population is captured by the first two field-free cation states. For reference, in the exact dressed-state basis, the residual population is about three orders of magnitude smaller than the populations in the first two dressed states. We therefore take $\tilde{N}=2$ in the parametrized semiclassical model, (12), which leads to the two-electron density

$$||\psi\rangle|^2 = \frac{\rho(r_2)}{2}\left|\gamma^d_1\tilde{\psi}^d_1(r_1) + \gamma^d_2 e^{i\left(S^s_{12}(r_2)+\Phi^d_{12}\right)}\tilde{\psi}^d_2(r_1)\right|^2, \tag{13}$$

with S^s_{12} and $\Phi^d_{12} = \Phi^d_2 - \Phi^d_1$ the stationary and ionization phase differences between the two (dressed) channels.

A. Ionization delay

From the expression of the stationary phase, (11), we note that the phase difference between the two ionization channels,

$$S^s_{12}(r_2) = \frac{\left[2\left(-\mathcal{E}r_N - I^n_p + I^d_{p_2}\right)\right]^{\frac{3}{2}} - \left[2\left(-\mathcal{E}r_N - I^n_p + I^d_{p_1}\right)\right]^{\frac{3}{2}}}{3\mathcal{E}},$$

is independent of the absolute time t. We have confirmed numerically that once the static-field-ionized wave packet has reached a given ionization coordinate r_2, the two-electron density remains constant at all later times. This ensures that we can reconstruct the ionization delay from the coordinate r_2, by providing a consistent reference from full TDSE computations: The charge migration dynamics in the cation, and its signature in the modulation of subsequent ionization, only depends on the time since the first ionization, i.e., how far the

ionized electron has traveled. Throughout the remainder of the paper we therefore omit the absolute time variable t in most equations.

In the leading-order expansion, the phase difference between the two channels becomes

$$S^s_{12}(r_2) \approx_{|r_2|\gg 1} \left(I^d_{p_2} - I^d_{p_1}\right)\tau_{\rm cl}.$$

This factorizes as the energy difference between the two dressed states multiplied by the classical ionization delay, (1). It corresponds to the fully classical picture for the ionized electron, where the two ionization channels have the same continuum dynamics and therefore the same accumulated phase. These cancel and the phase modulation is fully determined by the energy difference between the two ionization channels.

For higher-order results, we keep the full semiclassical expression and define the ionization delay as

$$\tau(r_2) = \frac{S^s_2(r_2) - S^s_1(r_2)}{I^d_{p_2} - I^d_{p_1}}. \tag{14}$$

In all figures, Eq. (14) is used to perform the conversion from the ionization coordinate r_2 to the delay τ in the analysis of our TDSE simulations. Physically, compared to the fully classical limit, (1), higher-order terms can be interpreted as accounting for channel-specific ionization conditions due to the different ionization barriers $I^n_p - I^d_{p_{1,2}}$ (see Sec. IV B).

We now have all the ingredients necessary to study charge migration following multichannel ionization in our $1+1D$ molecular model. More specifically, as a function of the ionization delay τ, (14), the electron density in the cation is given by

$$|\tilde{\psi}(r_1,\tau)|^2 = \frac{|\psi(r_1,r_2(\tau))|^2}{\rho(r_2(\tau))/2}. \tag{15}$$

We display the result for various delays in Fig. 3 (thick black curves; each panel corresponds to section ①–③ in other figures); a video of the charge migration is also available in the Supplementary Material [67]. It confirms the observations in Sec. II: Following multichannel ionization a migration of the charge is observed between the two molecular centers (vertical lines). Looking closely at the double-ionization dynamics ($r_1 \ll -1$) we see that a burst of ionization is generated following the full localization of the electron density downfield center (①), and the double-ionization channel is suppressed when the electron is delocalized over the two centers (③). This is a clear signature of the charge migration dynamics in the double-ionization oscillations, through the control it exercises on the release of the second electron (localization in the downfield molecular center).

B. Cation component representation basis

One could fit the results of the TDSE calculation as a means of extracting the parameters of the semiclassical model, (13). This all-at-once-fit strategy is unreliable, yielding unstable and sometimes unphysical results. Alternatively, and similarly to what would be done for systems where brute-force TDSE is not feasible, we have determined these parameters independently through physically reduced models, e.g., corresponding to the electronic structure of the cation for the different ionization

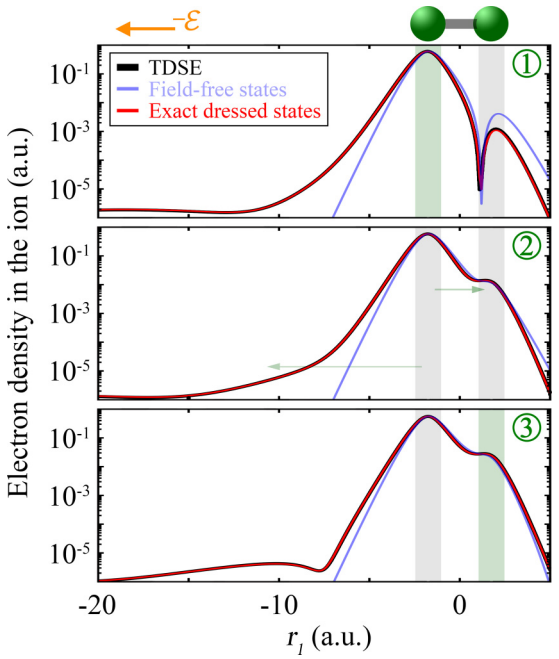

FIG. 3. Comparison of the electron density in the cation $2|\psi|^2/\rho$ from the TDSE vs our semiclassical model, with field-free and exact dressed ion states (see legend), for the section labeled in Figs 1 and 2. The associated video can be found in the Supplemental Material [67].

energies $I^d_{p_k}$. This method has proven successful, leading to well-defined (stable) parameters. We have checked the robustness of our ability to obtain these with changing electric-field and molecular parameters.

As discussed above, the most natural representation basis for the cation component is built from field-free eigenstates, as they are unambiguously defined by the cation component effective Hamiltonian $\hat{\mathcal{H}}_{N-1}$. The corresponding semiclassical electron density, with truncation order $\tilde{N} = 2$, is displayed by light-blue curves in Fig. 3. Compared with the TDSE reference (thick black curve), we see that this model reproduces very well the charge migration dynamics in the core region, around the molecular centers (vertical lines). Away from the core, however, the model fails to describe the (double-) ionization dynamics. These observations are confirmed in the lower panel in Fig. 1, where the semiclassical density (light-blue curve) reproduces very well the TDSE reference (thick black curve) in the upfield center ($r_1 = R/2$ set of curves) but completely fails to capture the modulation in the density away from the core, in the double-ionization region ($r_1 = -8$ a.u.). The failure to account for subsequent double ionization is hardly a surprise given the chosen basis of field-free states, which represent bound electrons. In order to capture double ionization one would probably have to expand drastically the representation basis with $\tilde{N} \gg 2$ and include, e.g., many Rydberg states.

The aforementioned failure to reproduce all of the full $1+1D$ TDSE dynamics is not to be put on the semiclassical model, (13), but solely on the choice of the cation component basis representation. Indeed, for comparison, we have performed a precise computation of the dc-field dressed states, including the distant—double-ionization—region from the core. We refer

to these as the "exact" dressed states throughout the paper. The resulting semiclassical prediction is displayed by thin red curves in the bottom panel in Fig. 1 and in Fig. 3. The results fall almost perfectly on top of the TDSE reference (thick black curves) and captures both the charge migration dynamics, following multichannel ionization, and the modulations it induces in subsequent (sequential) double ionization. Compared to the "natural" field-free-state representation, the exact dressed states can be heuristically interpreted as follows: First, one builds the effective cation Hamiltonian operator matrix $\tilde{\mathcal{H}}_{N-1}$ including many (Rydberg) states, so as to span distant regions from the core, to include subsequent ionization routes. Then one performs the diagonalization of the extended matrix to find the dressed states (as described in the introduction of Sec. IV). Finally, one performs the truncation to order $\tilde{N} = 2$, e.g., noting that the first two exact dressed states capture virtually almost all of the electron population in the cation [see Fig. 2(d)]. Compared to the field-free model described above, the inversion of the "Hamiltonian matrix diagonalization" and "truncation" steps has two main advantages: First, it offers a much more precise modeling; it quantitatively reproduces the full TDSE results, including the modulation in double ionization. Second, it keeps the number of dressed states involved in the model minimal, with only two effective channels here.

VI. CONCLUSION: BEYOND STATIC FIELDS

In conclusion, we have shown that even in the simplest case of a static (dc) field, ionization to more than one channel can lead to subsequent charge migration in the cation. A signature of this charge migration can be found in the modulation of subsequent double ionization, even though it happens through a sequential process; with a static field, recollision is not possible. Mathematically, the charge migration can be linked to the different rates at which each ionization channel accumulates phase and the resulting constructive and destructive interferences in the coherent superposition of involved cation states. Physically, the modulation can be understood in terms of the ionization delay-dependent localization of the electron density on the cation. In our case only the full localization of the electron in the downfield molecular center can lead to double ionization, while the double-ionization channel is suppressed when the electron is delocalized over the two centers.

By varying the internuclear distance R in our potential model of Eq. (3) (not shown)—which amounts to tuning the molecular properties of the target—we identify the two necessary ingredients for charge migration in the cation: (i) ionization to more than one dressed channel and (ii) spatial overlap between the dressed cation states, i.e., a coherent electron-hole wave packet in the cation. For small internuclear distances, dressed states strongly overlap spatially but ionization occurs in only one channel. On the other hand, with large internuclear distances significant ionization in both dressed channels is observed but they do not overlap spatially. In both cases, it leads to the disappearance of the charge migration dynamics described above. Here, it is important to note that charge migration is a coherent evolution of charge from one region of space to another. Charge migration can be distinguished from typical excitations due to the longer timescales needed for the larger body of charge to move. In a larger molecule, for example, charge migration would describe the motion of charge from one end to the other, whereas excitations would be dominated by transitions between nearby atoms.

Our analysis also provides a quantitative validation of semiclassical models for multichannel ionization and subsequent charge migration dynamics. This is particularly relevant given that such approaches have flourished in the past few years with the attempt to model, analyze, and identify charge migration in complex multiactive electron systems [7,11,22–25,43,54], where full *ab initio* TDSE computations are out of reach. We stress that the key to the success of the semiclassical model derivation was to rewrite the problem in a basis of dressed states, which effectively decouples the different ionization channels. Each can then be treated independently, similarly to well-known single-active-electron systems, and the overall coherence is only located in the ionization condition (as an initial-condition entanglement). Another by-product of the dressed-state formulation is that, after diagonalization of the matrix $\tilde{\mathcal{H}}_{N-1}$, the complexity of computations grows linearly with the number of dressed states. On the other hand, the complexity scales quadratically if one stays, e.g., in the field-free basis (the time propagator is a full matrix).

The comparison between models using reduced field-free states and exact dressed states with the $1+1D$ TDSE reference in Figs. 1 and 3 is also instructive for semiclassical models and analyses. For processes involving only a single ionized electron we see in our simulations that a reduced basis of field-free cation states is sufficient to describe the charge migration dynamics in the core region, with very good accuracy. On the other hand, if subsequent ionization or the dynamics in regions distant from the core are of interest, more care/refined states should be considered in order to account for them in the semiclassical approach.

Our main motivation for considering a static (dc) field is that it spatially separates ionization delays, and a single semiclassical trajectory is associated with each ionized electron coordinate (see also Sec. II). We used this property to reconstruct the ionization delay and, from there, the charge migration dynamics in the cation following multichannel ionization from full *ab initio* TDSE computations. This allowed us to quantitatively validate our semiclassical model, (13), and interpret the signature of charge migration in modulation of the double ionization. Almost all experiments in strong-field physics and attosecond science, however, use oscillating (ac) laser fields. Looking back at Fig. 1, we note that the charge migration period is about 14.5 a.u. (about 350 as). At this time scale, midinfrared lasers can be seen as a slowly varying electric field; in our example the period of the dynamics is about $1/20$ that of a 2-μm laser. In the sequential regime, i.e., neglecting recollision-induced double ionization, the wave-function expansion, (5), is not specific to dc fields and can equally well be applied to ac ones. From there, the main difference is that the cation component effective Hamiltonian operator $\hat{\mathcal{H}}_{N-1}$ now has an explicit time dependence. As a result the associated matrix $\tilde{\mathcal{H}}_{N-1}$ is finite-dimensional with *periodic* time-dependent coefficients. For such systems, the Floquet framework extends the notion of dressed eigenstates

[68] and can decouple them. For the ionized electron component, the dynamics of a continuum electron in an oscillating field has been repeatedly shown to be very well described by semiclassical models. This means that working in the Floquet basis offers the possibility of describing the system as a coherent superposition of decoupled—effectively single-active-ionized electron—channels. For such single-active-electron processes, QRS [63] has been shown to produce qualitatively and quantitatively more accurate results than its semiclassical counterparts. It therefore opens avenues to extending the technique to multichannel processes with oscillating fields.

ACKNOWLEDGMENTS

The authors thank L. F. DiMauro, T. T. Gorman, S. Hernandez, R. R. Jones, S. Khatri, T. D. Scarborough, and P. Sándor for enlightening discussions. This work was supported by US Department of Energy, Office of Science, Office of Basic Energy Sciences, under Award No. DE-SC0012462.

[1] P. Agostini and L. F. DiMauro, Rep. Prog. Phys. **67**, 813 (2004).
[2] P. B. Corkum and F. Krausz, Nat. Phys. **3**, 381 (2007).
[3] M. F. Kling and M. J. Vrakking, Annu. Rev. Phys. Chem. **59**, 463 (2008).
[4] F. Krausz and M. Ivanov, Rev. Mod. Phys. **81**, 163 (2009).
[5] F. Lépine, G. Sansone, and M. J. Vrakking, Chem. Phys. Lett. **578**, 1 (2013).
[6] M. J. J. Vrakking, Phys. Chem. Chem. Phys. **16**, 2775 (2014).
[7] J. P. Marangos, J. Phys. B **49**, 132001 (2016).
[8] M. F. Kling, C. Siedschlag, A. J. Verhoef, J. I. Khan, M. Schultze, T. Uphues, Y. Ni, M. Uiberacker, M. Drescher, F. Krausz *et al.*, Science **312**, 246 (2006).
[9] P. Eckle, A. N. Pfeiffer, C. Cirelli, A. Staudte, R. Dorner, H. G. Muller, M. Buttiker, and U. Keller, Science **322**, 1525 (2008).
[10] W. Li, X. Zhou, R. Lock, S. Patchkovskii, A. Stolow, H. C. Kapteyn, and M. M. Murnane, Science **322**, 1207 (2008).
[11] E. Goulielmakis, Z.-H. Loh, A. Wirth, R. Santra, N. Rohringer, V. S. Yakovlev, S. Zherebtsov, T. Pfeifer, A. M. Azzeer, M. F. Kling *et al.*, Nature **466**, 739 (2010).
[12] G. Sansone, F. Kelkensberg, J. F. Perez-Torres, F. Morales, M. F. Kling, W. Siu, O. Ghafur, P. Johnsson, M. Swoboda, E. Benedetti *et al.*, Nature **465**, 763 (2010).
[13] F. Kelkensberg, W. Siu, J. F. Pérez-Torres, F. Morales, G. Gademann, A. Rouzée, P. Johnsson, M. Lucchini, F. Calegari, J. L. Sanz-Vicario *et al.*, Phys. Rev. Lett. **107**, 043002 (2011).
[14] D. Shafir, H. Soifer, B. D. Bruner, M. Dagan, Y. Mairesse, S. Patchkovskii, M. Y. Ivanov, O. Smirnova, and N. Dudovich, Nature **485**, 343 (2012).
[15] J. Leeuwenburgh, B. Cooper, V. Averbukh, J. P. Marangos, and M. Ivanov, Phys. Rev. Lett. **111**, 123002 (2013).
[16] K. J. Schafer, B. Yang, L. F. DiMauro, and K. C. Kulander, Phys. Rev. Lett. **70**, 1599 (1993).
[17] P. B. Corkum, Phys. Rev. Lett. **71**, 1994 (1993).
[18] M. Lewenstein, P. Balcou, M. Y. Ivanov, A. L'Huillier, and P. B. Corkum, Phys. Rev. A **49**, 2117 (1994).
[19] P. Salieres, B. Carre, L. Le Deroff, F. Grasbon, G. Paulus, H. Walther, R. Kopold, W. Becker, D. Milosevic, A. Sanpera *et al.*, Science **292**, 902 (2001).
[20] A. D. Bandrauk, S. Chelkowski, and H. S. Nguyen, Int. J. Quant. Chem. **100**, 834 (2004).
[21] F. Remacle and R. D. Levine, Proc. Natl. Acad. Sci. USA **103**, 6793 (2006).
[22] O. Smirnova, Y. Mairesse, S. Patchkovskii, N. Dudovich, D. Villeneuve, P. Corkum, and M. Y. Ivanov, Nature **460**, 972 (2009).
[23] Y. Mairesse, J. Higuet, N. Dudovich, D. Shafir, B. Fabre, E. Mevel, E. Constant, S. Patchkovskii, Z. Walters, M. Y. Ivanov *et al.*, Phys. Rev. Lett. **104**, 213601 (2010).
[24] F. Calegari, D. Ayuso, A. Trabattoni, L. Belshaw, S. De Camillis, S. Anumula, F. Frassetto, L. Poletto, A. Palacios, P. Decleva *et al.*, Science **346**, 336 (2014).
[25] P. M. Kraus, B. Mignolet, D. Baykusheva, A. Rupenyan, L. Horny, E. F. Penka, G. Grassi, O. I. Tolstikhin, J. Schneider, F. Jensen *et al.*, Science **350**, 790 (2015).
[26] A. I. Kuleff, N. V. Kryzhevoi, M. Pernpointner, and L. S. Cederbaum, Phys. Rev. Lett. **117**, 093002 (2016).
[27] M. Lara-Astiaso, A. Palacios, P. Decleva, I. Tavernelli, and F. Martin, Chem. Phys. Lett. **683**, 357 (2017).
[28] J. Breidbach and L. S. Cederbaum, Phys. Rev. Lett. **94**, 033901 (2005).
[29] A. l'Huillier, L. A. Lompre, G. Mainfray, and C. Manus, Phys. Rev. A **27**, 2503 (1983).
[30] D. N. Fittinghoff, P. R. Bolton, B. Chang, and K. C. Kulander, Phys. Rev. Lett. **69**, 2642 (1992).
[31] K. Kondo, A. Sagisaka, T. Tamida, Y. Nabekawa, and S. Watanabe, Phys. Rev. A **48**, R2531 (1993).
[32] B. Walker, B. Sheehy, L. F. DiMauro, P. Agostini, K. J. Schafer, and K. C. Kulander, Phys. Rev. Lett. **73**, 1227 (1994).
[33] W. Becker and H. Rottke, Contemp. Phys. **49**, 199 (2008).
[34] C. F. de Morisson Faria and X. Liu, J. Modern. Opt. **58**, 1076 (2011).
[35] W. Becker, X. Liu, P. J. Ho, and J. H. Eberly, Rev. Mod. Phys. **84**, 1011 (2012).
[36] T. Weber, M. Weckenbrock, A. Staudte, L. Spielberger, O. Jagutzki, V. Mergel, F. Afaneh, G. Urbasch, M. Vollmer, H. Giessen *et al.*, Phys. Rev. Lett. **84**, 443 (2000).
[37] B. Feuerstein, R. Moshammer, D. Fischer, A. Dorn, C. D. Schröter, J. Deipenwisch, J. R. C. Lopez-Urrutia, C. Höhr, P. Neumayer, J. Ullrich *et al.*, Phys. Rev. Lett. **87**, 043003 (2001).
[38] A. Rudenko, K. Zrost, B. Feuerstein, V. L. B. de Jesus, C. D. Schröter, R. Moshammer, and J. Ullrich, Phys. Rev. Lett. **93**, 253001 (2004).
[39] T. Zuo, A. D. Bandrauk, and P. Corkum, Chem. Phys. Lett. **259**, 313 (1996).
[40] M. Meckel, D. Comtois, D. Zeidler, A. Staudte, D. Pavicic, H. C. Bandulet, H. Pepin, J. C. Kieffer, R. Doerner, D. M. Villeneuve *et al.*, Science **320**, 1478 (2008).
[41] M. Peters, T. T. Nguyen-Dang, E. Charron, A. Keller, and O. Atabek, Phys. Rev. A **85**, 053417 (2012).

[42] J. Itatani, J. Levesque, D. Zeidler, H. Niikura, H. Pepin, J. C. Kieffer, P. B. Corkum, and D. M. Villeneuve, Nature **432**, 867 (2004).
[43] S. Haessler, J. Caillat, W. Boutu, C. Giovanetti-Teixeira, T. Ruchon, T. Auguste, Z. Diveki, P. Breger, A. Maquet, B. Carre *et al.*, Nat. Phys. **6**, 200 (2010).
[44] S. Haessler, J. Caillat, and P. Salières, J. Phys. B. **44**, 203001 (2011).
[45] L. Young, D. A. Arms, E. M. Dufresne, R. W. Dunford, D. L. Ederer, C. Höhr, E. P. Kanter, B. Krässig, E. C. Landahl, E. R. Peterson *et al.*, Phys. Rev. Lett. **97**, 083601 (2006).
[46] L. Fechner, N. Camus, J. Ullrich, T. Pfeifer, and R. Moshammer, Phys. Rev. Lett. **112**, 213001 (2014).
[47] E. Runge and E. K. U. Gross, Phys. Rev. Lett. **52**, 997 (1984).
[48] S. J. A. van Gisbergen, F. Kootstra, P. R. T. Schipper, O. V. Gritsenko, J. G. Snijders, and E. J. Baerends, Phys. Rev. A **57**, 2556 (1998).
[49] M. Marques and E. Gross, Annu. Rev. Phys. Chem. **55**, 427 (2004).
[50] M. Lein and S. Kümmel, Phys. Rev. Lett **94**, 143003 (2005).
[51] S.-K. Son and S.-I. Chu, Phys. Rev. A **80**, 011403(R) (2009).
[52] N. T. Maitra, J. Chem. Phys. **144**, 220901 (2016).
[53] B. Augstein and C. F. de Morisson Faria, J. Mod. Opt. **58**, 1173 (2011).
[54] O. Smirnova and M. Ivanov, in *Attosecond and XUV Spectroscopy: Ultrafast Dynamics and Spectroscopy*, edited by T. Schultz and M. Vrakking (Wiley, New York, 2014), Chap. 7.8.
[55] J. Javanainen, J. H. Eberly, and Q. Su, Phys. Rev. A **38**, 3430 (1988).
[56] S. N. Pugliese, A. S. Simonsen, M. Førre, and J. P. Hansen, Phys. Rev. A **92**, 023424 (2015).
[57] F. Mauger, P. M. Abanador, K. Lopata, K. J. Schafer, and M. B. Gaarde, Phys. Rev. A **93**, 043815 (2016).
[58] R. Santra and A. Gordon, Phys. Rev. Lett. **96**, 073906 (2006).
[59] M. Spanner and S. Patchkovskii, Chem. Phys. **414**, 10 (2013).
[60] P. M. Kraus, O. I. Tolstikhin, D. Baykusheva, A. Rupenyan, J. Schneider, C. Z. Bisgaard, T. Morishita, F. Jensen, L. B. Madsen, and H. J. Wörner, Nat. Commun. **6**, 7039 (2015).
[61] M. D. Śpiewanowski, A. Etches, and L. B. Madsen, Phys. Rev. A **87**, 043424 (2013).
[62] M. D. Śpiewanowski and L. B. Madsen, Phys. Rev. A **89**, 043407 (2014).
[63] C. D. Lin, A.-T. Le, Z. Chen, T. Morishita, and R. Lucchese, J. Phys. B. **43**, 122001 (2010).
[64] M. V. Frolov, N. L. Manakov, T. S. Sarantseva, and A. F. Starace, J. Phys. B. **42**, 035601 (2009).
[65] C. Lanczos, Z. Phys. **62**, 518 (1930).
[66] R. J. Damburg and V. V. Kolosov, J. Phys. B **9**, 3149 (1976).
[67] See Supplemental Material at http://link.aps.org/supplemental/10.1103/PhysRevA.97.043407 for the associated video.
[68] V. Kapoor and D. Bauer, Phys. Rev. A **85**, 023407 (2012).